



ELSEVIER

Contents lists available at ScienceDirect

Applied Surface Science

journal homepage: www.elsevier.com/locate/apsusc

Full Length Article

Etching processes of transferred and non-transferred multi-layer graphene in the presence of extreme UV, H₂O and H₂

B.K. Mund^a, J.M. Sturm^{a,*}, W.T.E. van den Beld^a, C.J. Lee^b, F. Bijkerk^a^a Industrial Focus Group XUV Optics, MESA+ Institute of Nanotechnology, University of Twente, Enschede, the Netherlands^b Institute of Engineering, Fontys Hogescholen, Eindhoven, the Netherlands

ARTICLE INFO

Keywords:

Extreme Ultraviolet light
Hydrogen
Multi-layer graphene
Water
Oxidation

ABSTRACT

In this work we expose transferred multi-layer graphene (i.e. graphene separated from the substrate used for graphene growth and placed onto a carrier sample) to Extreme Ultraviolet light and water, in the presence of hydrogen. It is observed that graphene oxidizes by breaking down its aromatic structure into the enol form of 1,3-diketone. Furthermore, this oxidation is compared with studies on as-grown multi-layer graphene samples, which are shown to not oxidize. Our work shows that oxidation is most likely limited to a few layers of graphene at the interface between the graphene and the substrate onto which it is transferred. This is attributed to the presence of water, trapped during the transfer process, which is dissociated by secondary electrons from the substrate.

1. Introduction

Graphene, a 2D hexagonal lattice structure of carbon with covalently bound atoms, has been shown to possess a number of unique physical, thermal, and chemical properties [1–8]. Defect-free single layer graphene has been shown to be impermeable to gases [9,10], whereas defective multi-layer graphene has been shown to act as a membrane [11], and can be used to transfer protons through atomic defects [12]. Multi-layer graphene as a membrane has been proposed as a potential candidate for inexpensive water desalination [13], food packing [14], and anti-corrosion paint [15].

Optically, graphene is known to have highly desirable traits such as being transparent for both visible [16] and Extreme Ultraviolet (EUV) wavelengths [17]. These properties make graphene an attractive candidate for transparent conductive electrodes, such as flexible screens for smartphones and wearable devices, and EUV optics. High EUV transparency is very desirable, as most EUV optics require a layer to protect them from surface chemical processes, induced by high photon-energy radiation [18].

Single layer graphene, known for its low chemical reactivity when defect free, is highly susceptible to the formation of defects during growth, via chemical vapor deposition, and graphene transfer [19]. Defects may initiate oxidation and act as the nucleation point for further defect formation when graphene interacts with its environment [20,21]. Furthermore, the chemical reactivity of single layer graphene,

being one atomic layer thick, is highly dependent on the substrate on which it is transferred [22]. Using single layer graphene as a protective layer in chemically reactive environments may be unfavorable due to these drawbacks. Multi-layer graphene has been suggested as an alternative, which would still maintain most of the properties of single layer graphene, while being, in practice, less reactive and more robust due to its larger thickness [23].

The robustness of protective layers is of critical importance in EUV optical applications. Optical components are required to last the full lifetime (years) of beamline or imaging optics [18]. Therefore, it is important to reach a detailed understanding of the physical, chemical and electronic stability of multi-layer graphene and its reaction pathways in an EUV environment [24,25].

Previous research has shown that single-layer graphene in an EUV environment starts to oxidize when dosed with less than a monolayer of water (0.75 ML) and exposed in a partial pressure of 10^{-5} mbar of H₂ [25]. This oxidation was in the form of an enol form of 1,3-diketone which was characterized *in-situ* using Reflection Absorption Infrared Spectroscopy (RAIRS). It was concluded that diketone formation is due to the aromatic structure breakdown of graphene. The formation of the diketone was shown to saturate for prolonged exposure to water, EUV and H₂ under identical exposure conditions.

In this work, we further expand on 1,3-diketone formation and study its formation in multi-layer graphene under the same EUV exposure conditions using *in-situ* RAIRS characterization. We show that

* Corresponding author.

E-mail address: j.m.sturm@utwente.nl (J.M. Sturm).

<https://doi.org/10.1016/j.apsusc.2019.144485>

Received 22 July 2019; Received in revised form 23 September 2019; Accepted 21 October 2019

Available online 29 October 2019

0169-4332/ © 2019 Elsevier B.V. All rights reserved.

as-grown multi-layer graphene is resistant to oxidation when dosed with H₂O and exposed to EUV and H₂. However, transferred MLG is shown to oxidize. Oxidation is driven by the presence of water that is trapped at the interface between the graphene layer and the underlying substrate.

2. Experimental

The substrate for graphene growth consisted of 300 nm SiO₂, grown on a Si(1 0 0) wafer by dry oxidation at 1100 °C. Next, 70 nm of Mo was sputter deposited. Subsequently, multi-layer graphene was grown by chemical vapor deposition (CVD) at 1000 °C using a feedstock of Ar/H₂/CH₄ at 8 mbar in a cold-wall reaction chamber (VG Scienta at the NanoLab facilities at the University of Twente). The resultant graphene layer was then transferred onto an amorphous Si surface on a 10 mm × 10 mm substrate, using H₂O₂ as an etchant. The etchant dissolves the molybdenum film onto which the graphene is grown, resulting in a graphene sheet floating on top of the solution, which can be scooped with the substrate onto which the graphene has to be transferred [26]. This transfer process was performed without the use of any support polymer (e.g. PMMA) as is commonly used for the transfer of single layer graphene, enabling residue-free graphene transfer.

The substrates onto which MLG was transferred have a top layer of 22 nm of amorphous Si (aSi) on top of 9 nm of Mo deposited on a Si wafer (see Fig. 1). Both layers of Mo and aSi were sputter deposited, with their thicknesses calibrated by X-ray reflectivity measurements. Since the amorphous silicon is not protected from the environment after deposition, the top 1–2 nm of the surface is oxidized. The Mo layer was sandwiched between the aSi layer and the Si wafer to provide an infrared reflective sample, which is required to conduct *in-situ* RAIRS.

For EUV exposure experiments, the MLG-on-aSi sample was mounted on a 3-axis positioning manipulator in Ultra-High Vacuum conditions and maintained at a base pressure of 10⁻¹⁰ mbar. A K-type thermocouple is fixed to the sample to measure the surface temperature, and a Eurotherm temperature controller is used to control the surface temperature by radiative heating. Surface chemistry experiments, such as water dosing and Ar⁺ ion exposure, were conducted in the same experimental setup without breaking vacuum.

The chamber is equipped with RAIRS and Temperature Programmed Desorption (TPD) spectroscopy [27]. RAIRS spectra are measured at grazing incidence using a Fourier Transform Infrared (FTIR) spectrometer (Bruker Vertex 70 V), which is equipped with a liquid N₂ cooled detector. Each IR spectrum is summed over 256 scans with a resolution of 4 cm⁻¹. Background and sample scans were recorded at the lowest possible stable surface temperature (~85 K). The sample is placed ~1 mm away from the aperture of a Hiden Analytical 3F/PIC quadrupole mass spectrometer to obtain TPD spectra. Deionized water is dosed on the surface using a retractable quartz tube connected via a pinhole. Surface coverage is calibrated against reference TPD spectra obtained from a clean Ru(0001) surface [28].

The chamber is also attached to a Xe plasma discharge Extreme Ultraviolet source (Philips EUV Alpha Source 2) with a repetition rate of 500 Hz. EUV light is filtered from the source using a Mo/Si reflective mirror (55% reflectivity at 13.5 nm) and transmission through a Si/Mo/Zr membrane (35% transmission at 13.5 nm) [25,29–31]. This results in a total transmission of 19.25% at 13.5 nm with a FWHM of 0.2 nm. The

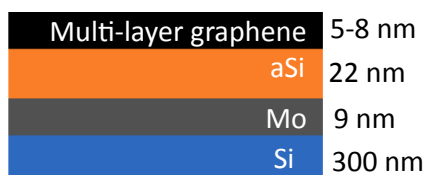


Fig. 1. Schematic representation of multi-layer stack used for transferred multi-layer graphene experiments.

beam has a Gaussian profile (FWHM = 3 mm) with an intensity of 35–55 mW/cm², corresponding to a dose of 90–110 μJ/cm² per pulse.

The experimental procedure is, unless otherwise stated, as follows: a background IR spectrum at 85 K is recorded, the surface is dosed with 0.75 ML of water and exposed to EUV with different partial pressures of hydrogen (either 1 × 10⁻⁵ mbar or 1 × 10⁻⁴ mbar, unless otherwise stated). Further IR spectra are recorded at 10 min intervals until the end of the 60 min of EUV + H₂ exposure. Finally, TPD is performed by heating the surface to 450 K at a rate of 1 K/s.

X-ray Photoelectron Spectroscopy (XPS) measurements are performed *ex-situ* using monochromatic Al-Kα radiation, employing a ThermoFisher Theta Probe with a beam spot size of about 1 mm in diameter. Scanning Electron Microscopy (also *ex-situ*) measurements were performed with a high resolution SEM (HR-SEM) using a voltage of 2 kV, with a point resolution of 1.2 nm.

3. Results and discussion

3.1. As grown multi-layer graphene on Mo

Previous results, mentioned in the introduction and reproduced in Fig. 2, line (a), show the RAIRS data of a transferred single layer graphene when exposed to EUV, H₂ (10⁻⁵ mbar) and H₂O (0.75 ML) for 60 min. Apart from the water peaks (O-H stretch, O-H bend and libration), we see a peak at ~2480 cm⁻¹, corresponding to the formation of the enol form of 1,3-diketone. This indicates oxidation of the graphene layer and degradation of its aromatic structure [25].

For this work, an as-grown ~6 nm thick multi-layer graphene sample was first dosed with 0.75 ML of H₂O and then exposed to EUV at H₂ partial pressures ranging from 1 × 10⁻⁵ to 1 × 10⁻³ mbar. Prior to exposure, a defect density (I(D)/I(G)) of 0.11 was measured using Raman spectroscopy, which corresponds to an inter-defect distance of > 24 nm [32]). As shown in Fig. 2, line (b), with a partial pressure of up to 10⁻³ mbar of H₂, there is no increase in the spectral region associated with keto-enol formation, even after 60 min of exposure. This indicates that as-grown multi-layer graphene is more resistant to oxidation compared to transferred single-layer graphene.

The absence of the expected formation of a keto-enol peak on as-grown multi-layer graphene might be explained by a lower defect density for the multi-layer graphene sample. The previously investigated single layer graphene samples (line (a) in Fig. 2) were reported to have an I(D)/I(G) ratio on the order of 0.7 and an inter-defect distance of 20 nm. To test this hypothesis, a graphene layer with a higher initial defect density was exposed under identical exposure conditions. In this experiment, an as-grown multilayer graphene stack, ~6 nm thick, with a higher defect ratio of I(D)/I(G) = 0.31 was used. Again, RAIRS shows that there is no formation of a keto-enol peak when the water dosed surface (0.75 ML) is exposed to EUV at a relatively high partial pressure of H₂ at 10⁻³ mbar (Fig. 2, line (c)). The RAIRS spectra indicate, therefore, that no oxidation is taking place in the MLG structure. This conclusion is supported by XPS measurements, which show no increase in the C-O group contribution to the C1s, nor any significant change in the O1s signal. Furthermore, no changes in C1s sp² to sp³ ratio were observed. In contrast, for transferred single layer graphene, changes to both the sp² to sp³ ratio and the C-O group contribution to C1s were observed under these exposure conditions [25].

To confirm that defect density plays little role in oxidation, the defect ratio was modified during exposure using Ar⁺ sputtering. The graphene surface was exposed to Ar ions with an energy of 2.8 keV for a total of 35 min (813 μC/cm²) which is enough to remove a monolayer of graphene, according to the Bohdanský-Yamamura [33] model. Similar to earlier results, there is no evidence of keto-enol formation in RAIRS for as-grown MLG dosed with water and exposed to EUV and H₂ (Fig. 2, line (d)). Furthermore, while *ex-situ* experiments, such as Raman spectroscopy, showed an increase in the I(D)/I(G) ratio from 0.31 to 0.71 after sputtering and exposure, this did not correspond to

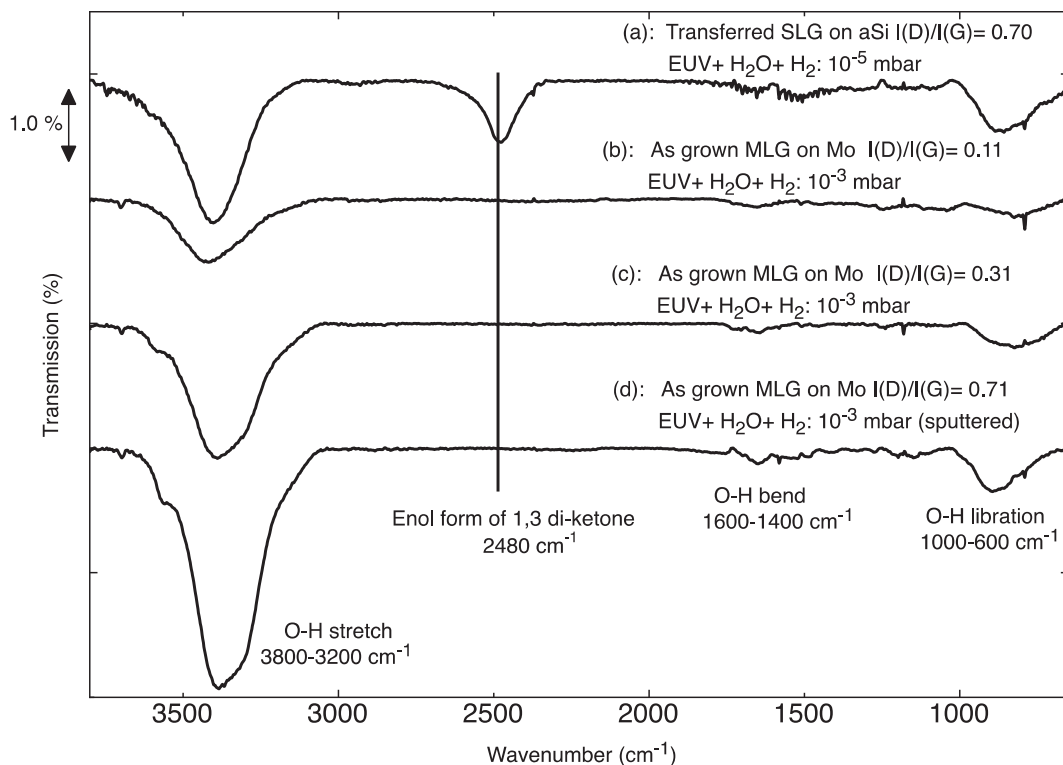


Fig. 2. RAIRS spectra after 60 min of exposure to H₂O, EUV and H₂ that show damaging of SLG (line (a)) at lower H₂ pressures in the form of enol formation (2480 cm⁻¹) in contrast to MLG which does not show any enol formation even at higher pressures (lines (b-d)). The hydrogen pressures and I(D)/I(G) ratios are mentioned in the plot. The peaks present in the spectra correspond to different O-H modes of adsorbed water [28]: stretch (3200–3800 cm⁻¹), bend (1400–1600 cm⁻¹) and libration (600–100 cm⁻¹).

noticeable changes in the overall sp² to sp³ ratio after exposure or change in the C-O peak, which would reflect an oxidized MLG.

RAIRS spectra of the O-H stretch peak (3800–3200 cm⁻¹), originating from water adsorbed on the sample, show variations in intensity between different samples and exposures. The reason for this is twofold: (i) the residual water pressure during exposure depends on the exposure history of the vacuum system and (ii) depending on initial surface condition of the graphene, the orientation of the adsorbed water may change, so that a different fraction of the O-H stretches is out-of-plane (the in-plane mode is dipole forbidden in reflection mode). However, it should be noted that prior to each EUV exposure, the sample was reproducibly dosed with 0.75 ML of water. Since water in direct contact with the surface is expected to have the highest potential contribution to oxidation of the graphene, possible variations in adsorption of water from residual gas are considered less important compared to initially dosed water.

3.2. Transferred multi-layer graphene onto amorphous Si

Exposures were also performed for multi-layer graphene which was transferred (I(D)/I(G) = 0.31 after transfer) to an amorphous Si layer. As described earlier, the surface was dosed with 0.75 ML of water, and exposed to EUV with different partial pressures of hydrogen. As shown in Fig. 3, a keto-enol peak [34] (2300–2700 cm⁻¹) forms when the water dosed surface is exposed to EUV at a partial pressure of 1 × 10⁻⁴ mbar of H₂. Similar to the case for SLG, the keto-enol peak (2484 cm⁻¹) is visible after 10 min of exposure to H₂O, EUV and H₂.

The increasing peak intensity for longer exposure times suggests that 1,3-diketone continues to form during exposure, likely at the edges of graphene grain boundaries, which are relatively more hydrophilic and reactive than mid-grain points on the graphene layer [35]. Later in this section we discuss differences between transferred and non-transferred graphene samples that likely explain the difference in reactivity.

The formation of this peak is seen in more detail in Fig. 4, which displays RAIRS spectra after sequential exposures of the same sample (on the same spot) at different H₂ partial pressures. Curve I shows that the keto-enol peak becomes visible when the H₂ partial pressure is 1 × 10⁻⁵ mbar. Firstly, the peak continues to grow over 60 min with peak intensity at 2467 cm⁻¹. Secondly, after increasing the partial pressure of H₂ to 10⁻⁴ mbar (curve II), the keto-enol peak is observed to grow faster, and the peak intensity shifts to 2490 cm⁻¹. (Note that a new background spectrum was taken before each exposure step. The RAIRS signal thus only corresponds to molecular groups formed during each exposure run.) Thirdly, in curve III, where the exposure is repeated at 10⁻⁵ mbar H₂, we see that the growth rate of the keto-enol peak is slower compared to the previous exposure at 10⁻⁵ mbar H₂ (curve I). Finally, as the experiment conditions from curve II are repeated again, curve IV shows that the rise in peak intensity is lower compared to curve II.

A comparison of the growth of the keto-enol peak intensity for these different experiments is displayed in Fig. 5, where the peak intensity has been plotted against EUV exposure time. From Fig. 5 it is observed that the growth of the keto-enol peak for curve I (EUV + H₂ at 10⁻⁵ mbar) starts at 0.002%/min, while the rate of keto-enol growth increases to 0.014%/min when the hydrogen partial pressure is increased to 10⁻⁴ mbar (curve II). Finally, repeating/continuing the exposure experiments results in curve III and IV, with growth rates of 0.001%/min and 0.006%/min respectively, indicating that the growth rate of keto-enol formation is indeed decreasing with exposure time.

XPS data for a photoelectron take off angle of 34° (with respect to the surface normal) has been compared for transferred unexposed graphene and graphene after EUV and H₂ exposure in Fig. 6. Table 1 quantifies the spectral components seen in the XPS data. The C1s sp² and sp³ peak percentages before and after exposure fall within margins of error of each other, indicating that the graphene layer has remained unchanged after EUV exposure up to the information depth of XPS,

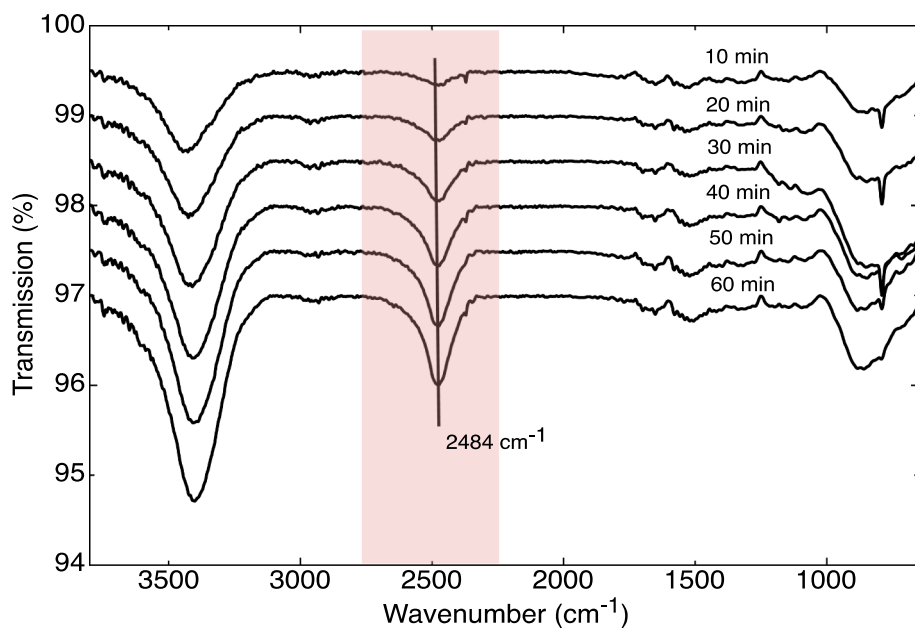


Fig. 3. Keto-enol formation ($2300\text{--}2700\text{ cm}^{-1}$) seen in transferred multi-layer graphene dosed with water (0.75 ML) and exposed to EUV with a partial pressure of 10^{-4} mbar of H_2 . The other peaks shown correspond to different O-H modes of adsorbed water: stretch ($3200\text{--}3800\text{ cm}^{-1}$), bend ($1400\text{--}1600\text{ cm}^{-1}$) and libration ($600\text{--}100\text{ cm}^{-1}$) [28].

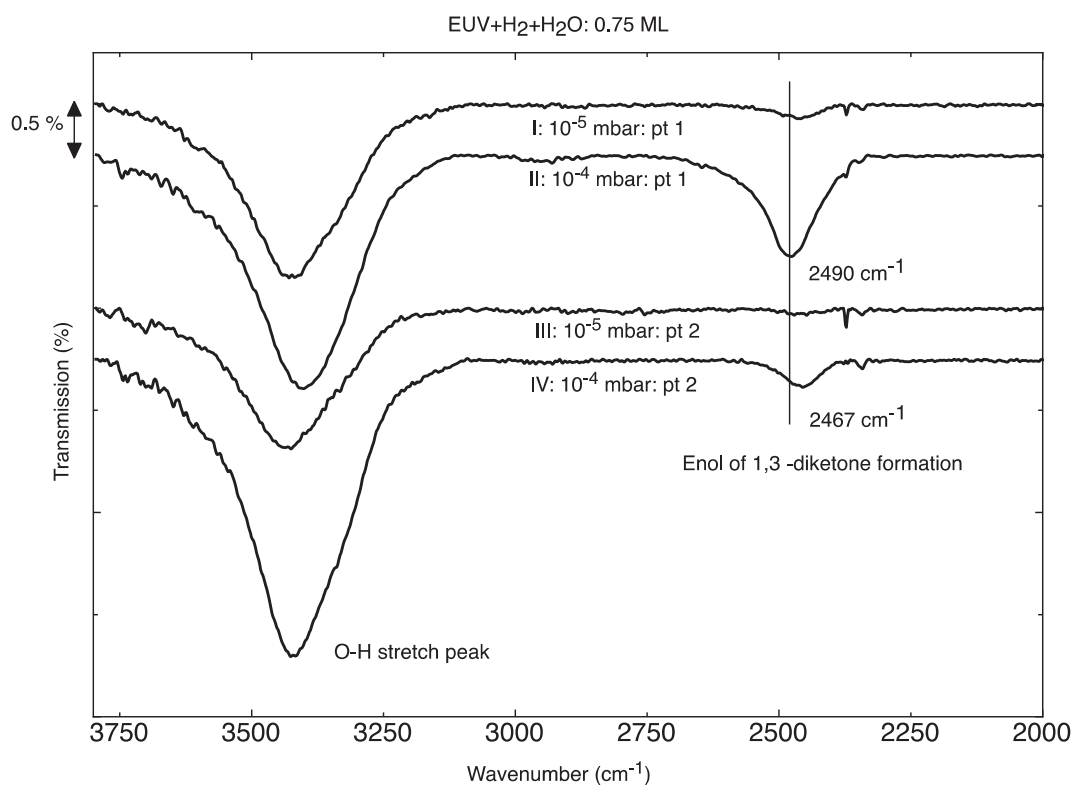


Fig. 4. Formation of keto-enol peak in a transferred MLG stack on aSi seen around $\sim 2400\text{--}2500\text{ cm}^{-1}$, with EUV and H_2O at different partial pressures of H_2 , after 60 min of exposure. Also, O-H stretches of adsorbed water ($3200\text{--}3400\text{ cm}^{-1}$) are seen. The experiments are done sequentially from I to IV, with a new background taken before every experiment.

which is about 5 nm for carbon [36]. Also, a Si 2p percentage around 1 at.% is detected before and after exposure. The silicon signal may be due to the Si substrate, which is on the edge of detection by the XPS, because the graphene layer is almost as thick ($\sim 5\text{--}8\text{ nm}$) as the information depth of the XPS. Furthermore, due to manufacturing defects, the graphene layer has holes that account for 2–3% of the total surface area. The presence of holes results in a photoelectron signal from the Si substrate. This is further discussed in the section below.

In our previous work on single layer graphene exposed to H_2O , EUV

and H_2 , changes in the sp^2 and sp^3 peaks were easily observable by eye [25]. In the case of multilayer graphene, possible chemical changes in the topmost monolayers are expected to be less visible due to the background signal from the graphene layers below. We also confirmed that no detectable changes in the C1s peak were observed for a more grazing angle of 72° with respect to the sample normal. If diketone formation occurred at the upper-most surface, the absolute increase in sp^3 peak area of the C1s peak should be similar to our previous EUV exposure experiments on single-layer graphene, where 12 at.% of $\text{sp}^3\text{ C}$

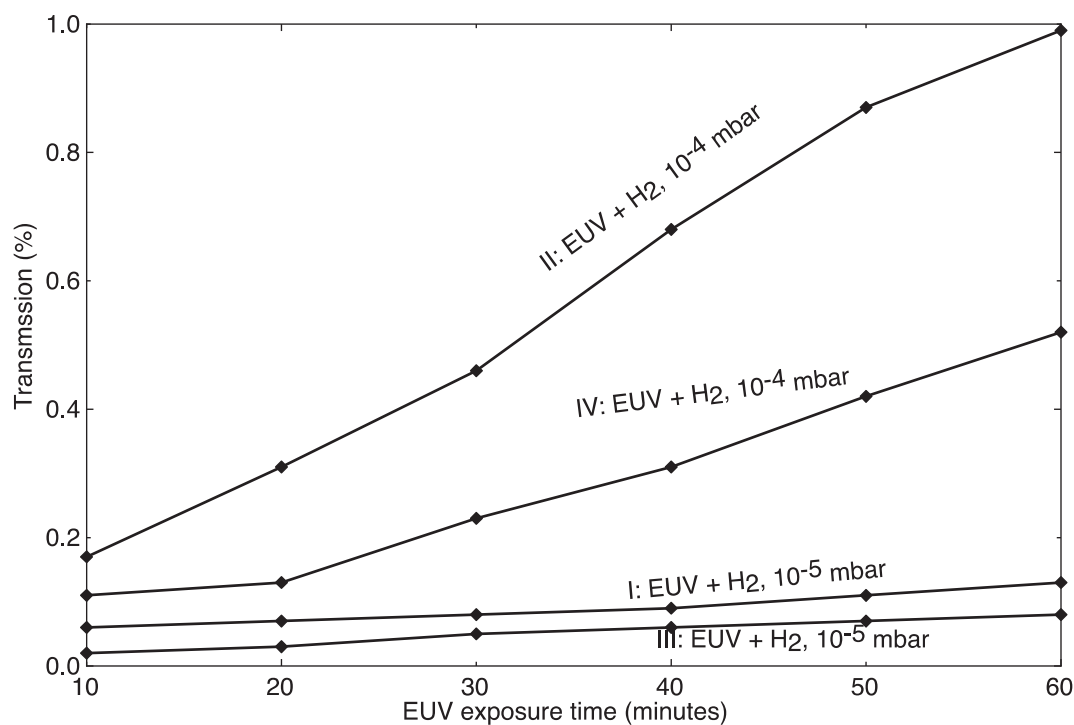


Fig. 5. Keto-enol peak intensity (negative transmission) plotted against EUV and H₂ exposure time for subsequent exposures at different hydrogen partial pressures for a transferred MLG stack on aSi. Exposures were conducted in the order from I to IV at indicated H₂ partial pressures. A background spectrum is subtracted at the beginning of each time-series.

was observed [25]. Analysis of the peak fitting indicates that the same increase in sp³ peak area as observed for damaged SLG would be detectable even if deeper graphene layers are not damaged. Moreover, it should be noted that no increase in the concentration of oxygen (based on the O 1s peak) was observed, which is an additional indication that no oxidation of the graphene is detectable within the information depth of XPS.

Based on the absence of oxidized graphene in the XPS signal, we conclude that the keto-enol oxidation observed in RAIRS is most likely originating from the interface between the graphene and the Si, which cannot be characterized by XPS.

SEM images for the transferred multi-layer graphene before and after exposure are shown in Fig. 7. As seen in the pictures, multiple holes are visible in the graphene layer. These holes are mostly around ~100 nm in diameter, with largest holes being ~300 nm in diameter. The smaller hole sizes (< 50 nm) are quantified in Fig. 8. Furthermore, the holes are through the depth of the graphene layer, exposing the Si substrate to the environment above the graphene layer, which was confirmed after looking at a cross section of a graphene layer in the SEM, as seen in Fig. 9.

Comparing a set of 10 images (field-of-view of 3 × 2.5 μm²) taken before and after exposure to EUV and H₂, we find that the number of holes less than 50 nm in diameter increases after exposure, whereas larger holes (> 50 nm) remain largely unaffected by EUV exposure. This has been quantified in Fig. 8, where we see that the average hole density for MLG before exposure is ~2.41 holes/μm² (σ = 0.25), which increases to ~3.90 holes/μm² (σ = 0.39) after exposure. Furthermore, we see a slight increase in hole percentage to total graphene area (as pictured in Fig. 7) from 2.21% before exposure to 2.68% after exposure. This increase in holes is most likely caused by oxidation of MLG and the breakdown of the graphene layer [37].

The cross-section of transferred multi-layer graphene in Fig. 9 shows that the graphene film retains the rough grain structure of the Mo film it was grown on. As a result, the film rests on the aSi surface with an irregular waviness of approximately 32 nm peak-valley. This waviness

could result in water being physisorbed between the MLG and aSi surface during the transfer process, with further water being introduced (via holes) during dosing and exposures. As a result, large amounts of water can remain trapped between the graphene layer and the substrate, which may dissociate into reactive species such as OH⁻ and H⁺ during EUV exposure [37]. This could support the fact that EUV photons react with water molecules, resulting in a trapped energy high enough to break C = C bonds and form small holes in the graphene layer.

Finally, the difference in EUV-induced secondary electron yield between graphene and the aSi substrate can contribute to the different reactivity of as-grown and transferred multilayer graphene. Carbon has a reasonably low secondary electron yield δ at 92 eV (13.5 nm) (δ = 0.37) as compared to the underlying substrate such as Si (δ = 0.74) or Mo (δ = 0.87) [38,39]. This means that water trapped between graphene and the a-Si substrate has a higher probability to be dissociated, resulting in production of O radical species, compared to water adsorbed onto the graphene surface.

4. Summary and conclusions

Previously it has been shown that single layer graphene sheets, as-grown or transferred, are likely to oxidize and form defects when introduced to an EUV environment in the presence of water and hydrogen [24,25,37]. This oxidation could be observed with RAIRS through the formation of keto-enol groups. In this work, we show that as grown multi-layer graphene is resistant to oxidation under the same exposure conditions up to 10⁻³ mbar of partial pressure of H₂. On the contrary, transferred MLG does show evidence of oxidation in RAIRS similar to SLG. Since the employed transfer process is polymer free, we can exclude that keto-enol formation occurs due to polymer residues such as PMMA. Two factors are identified as likely cause for the difference between as-grown and transferred MLG: firstly, MLG conforms to the grain boundaries of the Mo growth substrate, so EUV induced reactions with water can only take place on the topmost layers of the

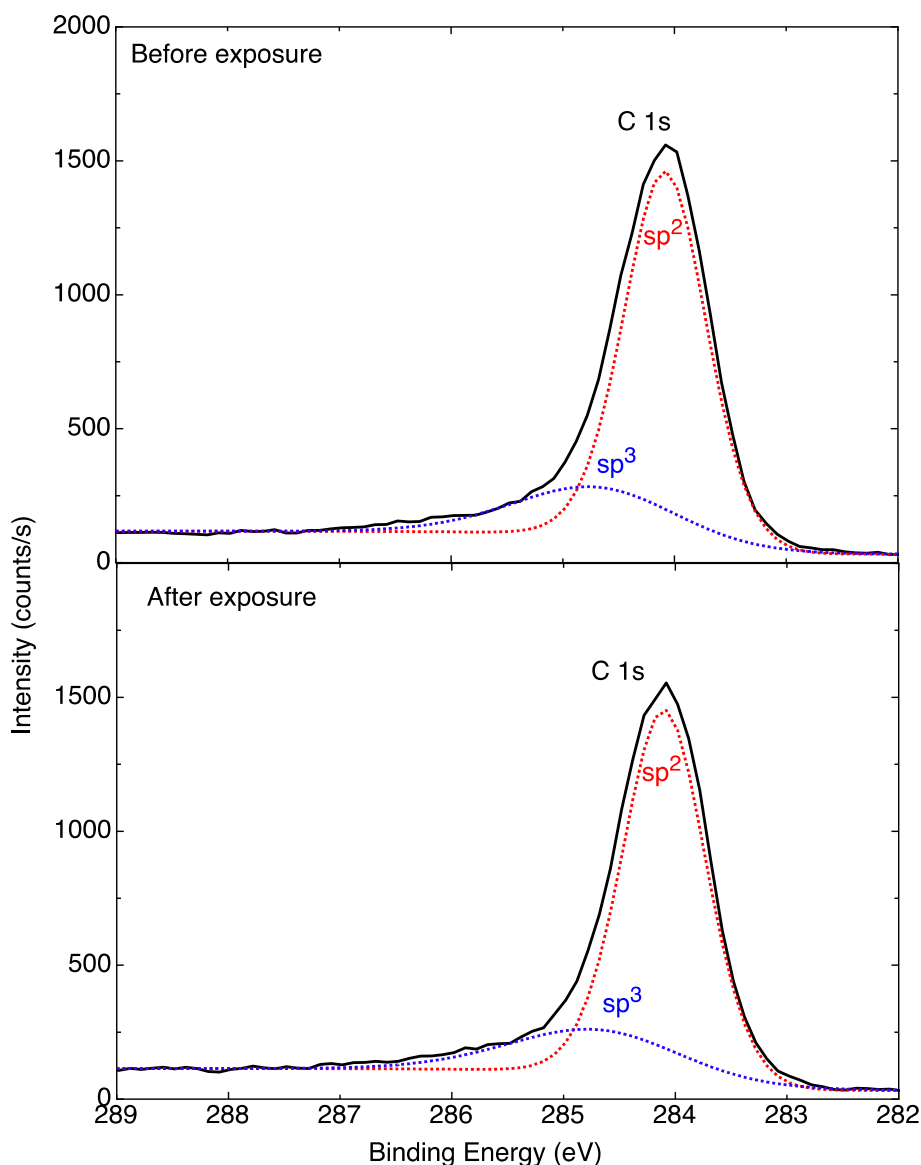


Fig. 6. The C1s peak in XPS for transferred multi-layer graphene before and after exposures (Figs. 4–5) to EUV.

Table 1

Atomic concentrations of spectral components of C 1s peak (C1s O, sp^2 and sp^3 , sp^2 FWHM), O 1s peak, Si 2p and oxidized Si 2p before and after exposure to multiple doses of EUV, H_2O and H_2 .

Name	Unexposed graphene (at %)	Exposed graphene (at %)
C 1s O/ tail sp^2 carbon	2.4 ± 0.2	1.21 ± 0.1
C1s sp^2	76 ± 7.5	76 ± 7.5
C1s sp^3	18.7 ± 2.0	19.9 ± 2.0
O1s	2.0 ± 0.2	1.45 ± 0.2
Si2p ox	0.42 ± 0.1	0.47 ± 0.1
Si2p elemental	1.02 ± 0.1	0.95 ± 0.1
C1s sp^2 FWHM (eV)	0.90 ± 0.1	0.90 ± 0.1

graphene. Secondly, the low EUV-induced secondary electron yield of carbon (graphene) reduces the generation of reactive O species from water adsorbed on MLG. The MLG thickness is larger than the secondary electron mean free path [36], thus, secondary electrons generated in the Mo substrate cannot reach adsorbed water on the graphene surface. This is in contrast to the case for single-layer graphene on a substrate with a relatively high SE yield, where the thickness of the graphene is smaller than the electron mean free path.

XPS data shows that graphene oxidation does not occur at the top surface of the graphene layer, leading to the conclusion that oxidation must occur at the interface between the graphene and the aSi. SEM pictures indicate that the transferred graphene is not conformal with the surface, which could result in trapped water during transfer and/or exposure, potentially leading to oxidation of the graphene when irradiated by EUV photons. Water trapped at the graphene-substrate interface is exposed to the relatively higher flux of secondary electrons from the substrate and is, thereby, more likely to initiate oxidation. SEM pictures of exposed transferred MLG show formation of additional small holes (< 50 nm in diameter), similar to previous reports on EUV exposed SLG [37].

Declaration of Competing Interest

We declare that we have no conflict of interest.

Acknowledgements

This research is supported by the Dutch Technology Foundation STW (project number 140930), which is part of the Netherlands

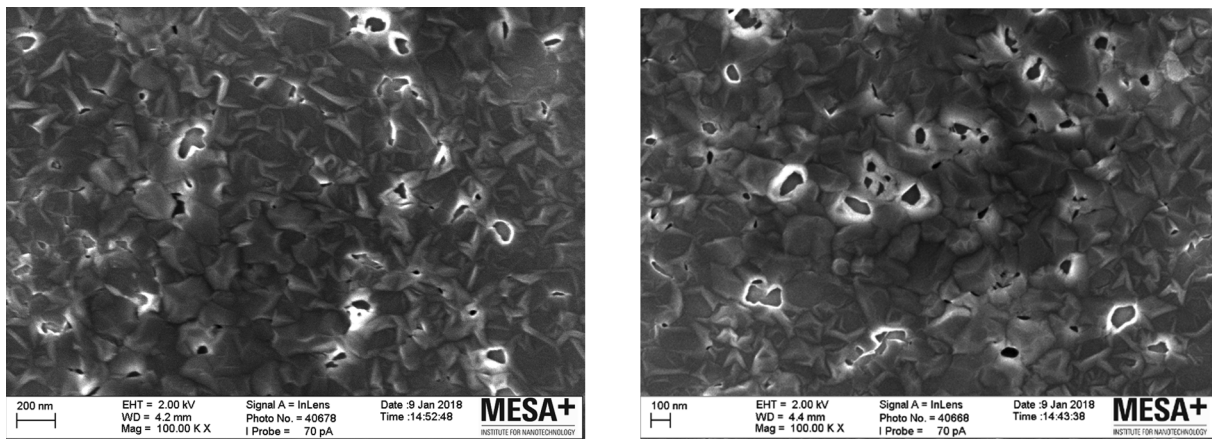


Fig. 7. SEM micrographs of transferred multi-layer graphene (a) unexposed and (b) exposed to EUV and H₂.

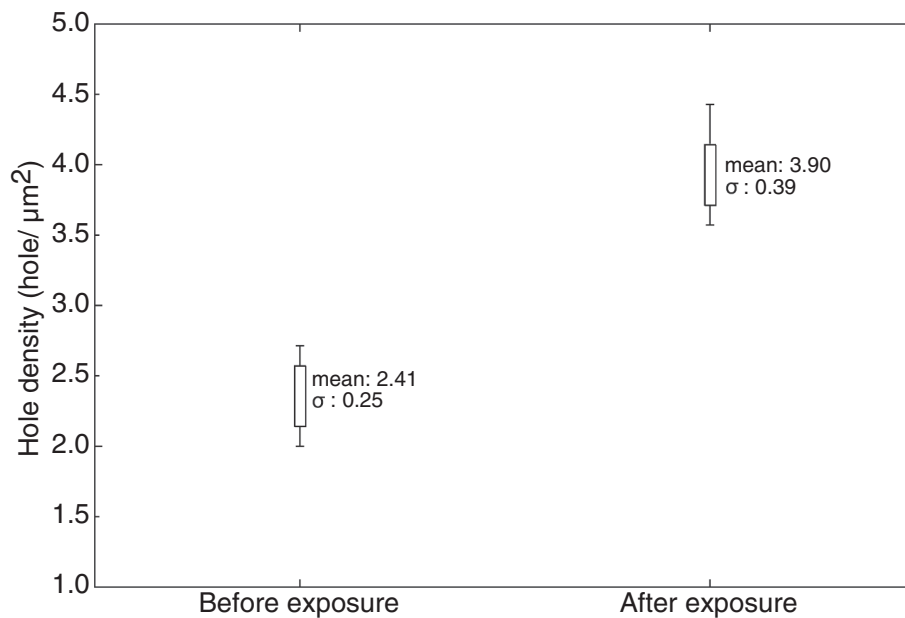


Fig. 8. Comparison of the density of holes less than 50 nm in diameter seen in transferred MLG (in field-of-view = $3 \times 2.5 \mu\text{m}^2$) in a set of 10 images before and after exposure to EUV and H₂.

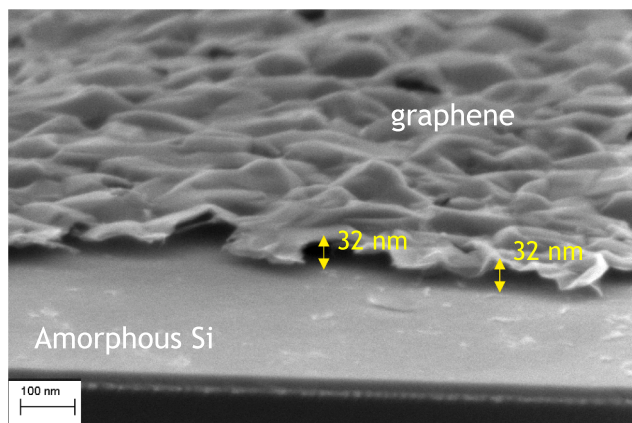


Fig. 9. Cross-section of exposed transferred MLG on amorphous Si, displaying the morphology of graphene on the transferred surface. The distance between the graphene layer and aSi surface is also indicated.

Organization for Scientific Research (NWO), and partly funded by the Ministry of Economic Affairs as well as ASML and ZEISS. We also acknowledge the financial and facility contributions by ASML, ZEISS, Malvern Panalytical, and the Province of Overijssel through the Industrial Focus Group XUV Optics at the MESA + Institute, University of Twente. The authors would like to thank Dr. Robbert van de Kruijs and Mr. Theo van Oijen for preparation of substrates, Mr. Parikshit Phadke for Ar⁺ sputtering calculations, all at the University of Twente, and Mr. Luc Stevens, Mr. John de Kuster and Mr. Goran Milinkovic at ASML for technical support.

References

- [1] A.K. Geim, K.S. Novoselov, The rise of graphene, *Nat. Mater.* 6 (2007) 183–191.
- [2] A.K. Geim, Graphene: status and prospects, *Science* 324 (2009) 1530–1534.
- [3] S. Hu, M. Lozada-Hidalgo, F.C. Wang, A. Mishchenko, F. Schedin, R.R. Nair, E.W. Hill, D.W. Boukhvalov, M.I. Katsnelson, R.A.W. Dryfe, I.V. Grigorieva, Y.H. Wu, A.K. Geim, Proton transport through one-atom-thick crystals, *Nature* 516 (2014) 227.
- [4] K.S. Novoselov, D. Jiang, F. Schedin, T.J. Booth, V.V. Khotkevich, S.V. Morozov, A.K. Geim, Two-dimensional atomic crystals, *Proc. Natl. Acad. Sci. USA* 102 (2005) 10451–10453.
- [5] C. Lee, X. Wei, J.W. Kysar, J. Hone, Measurement of the elastic properties and

- intrinsic strength of monolayer graphene, *Science* 321 (2008) 385–388.
- [6] M. Han, B. Özyilmaz, Y. Zhang, P. Kim, Energy band-gap engineering of graphene nanoribbons, *Phys. Rev. Lett.* 98 (2007) 206805.
- [7] P. Avouris, Graphene: electronic and photonic properties and devices, *Nano Lett.* 10 (2010) 4285.
- [8] K.I. Bolotin, K.J. Sikes, Z. Jiang, M. Klima, G. Fudenberg, J. Hone, P. Kim, H.L. Stormer, Ultrahigh electron mobility in suspended graphene, *Solid State Commun.* 146 (2008) 351–355.
- [9] V. Berry, Impermeability of graphene and its applications, *Carbon* 62 (2013) 1–10.
- [10] J.S. Bunch, S.S. Verbridge, J.S. Alden, A.M. van der Zande, J.M. Parpia, H.G. Craighead, P.L. McEuen, Impermeable atomic membranes from graphene sheets, *Nano Lett.* 8 (2008) 2458–2462.
- [11] R.K. Joshi, P. Carbone, F.C. Wang, V.G. Kravets, Y. Su, I.V. Grigorieva, H.A. Wu, A.K. Geim, R.R. Nair, Precise and ultrafast molecular sieving through graphene oxide membranes, *Science* 343 (2014) 752–754.
- [12] J.L. Achtyl, R.R. Unocic, L. Xu, Y. Cai, M. Raju, W. Zhang, R.L. Sacci, I.V. Vlassiok, P.F. Fulvio, P. Ganesh, D.J. Wesolowski, S. Dai, A.C.T. van Duin, M. Neurock, F.M. Geiger, Aqueous proton transfer across single-layer graphene, *Nat. Commun.* 6 (2015) 6539.
- [13] S. Homaeigohar, M. Elbahri, Graphene membranes for water desalination, *NPG Asia Mater.* 9 (2017) e427.
- [14] S. Seethamraju, S. Kumar, K.B. B, G. Madras, S. Raghavan, P.C. Ramamurthy, Million-fold decrease in polymer moisture permeability by a graphene monolayer, *ACS Nano*, 10 (2016) 6501–6509.
- [15] L. Kyhl, S.F. Nielsen, A.G. Čabo, A. Cassidy, J.A. Miwa, L. Hornekaer, Graphene as an anti-corrosion coating layer, *Faraday Discuss.* 180 (2015) 495–509.
- [16] R.R. Nair, P. Blake, A.N. Grigorenko, K.S. Novoselov, T.J. Booth, T. Stauber, N.M.R. Peres, A.K. Geim, Fine structure constant defines visual transparency of graphene, *Science* 320 (2008) 1308–1308.
- [17] B.L. Henke, E.M. Gullikson, J.C. Davis, X-ray interactions: photoabsorption, scattering, transmission, and reflection at $E = 50\text{--}30,000$ eV, $Z = 1\text{--}92$, *At. Data Nucl. Data Tables* 54 (1993) 181–342.
- [18] T.E. Madey, N.S. Faradzhev, B.V. Yakshinskiy, N.V. Edwards, Surface phenomena related to mirror degradation in extreme ultraviolet (EUV) lithography, *Appl. Surf. Sci.* 253 (2006) 1691.
- [19] D.-E. Jiang, B.G. Sumpter, S. Dai, Unique chemical reactivity of a graphene nanoribbon's zigzag edge, *J. Chem. Phys.* 126 (2007) 134701.
- [20] L.L. Liu, M.Q. Qing, Y.B. Wang, S.M. Chen, Defects in graphene: generation, healing, and their effects on the properties of graphene: a review, *J. Mater. Sci. Technol.* 31 (2015) 599–606.
- [21] P.A. Denis, F. Iribarne, Comparative study of defect reactivity in graphene, *J. Phys. Chem. C* 117 (2013) 19048–19055.
- [22] T. Tsukamoto, K. Yamazaki, H. Komurasaki, T. Ogino, Effects of surface chemistry of substrates on Raman spectra in graphene, *J. Phys. Chem. C* 116 (2012) 4732–4737.
- [23] D.D. Levin, I.I. Bobrinetskiy, A.V. Emelianov, V.K. Nevolin, A.V. Romashkin, V.A. Petuhov, Surface functionalization of single-layer and multilayer graphene upon ultraviolet irradiation, *Semiconductors* 50 (2016) 1738–1743.
- [24] A. Gao, P.J. Rizo, E. Zoethout, L. Scaccabarozzi, C.J. Lee, V. Banine, F. Bijkerk, Extreme ultraviolet induced defects on few-layer graphene, *J. Appl. Phys.* 114 (2013) 044313.
- [25] B.K. Mund, J.M. Sturm, C.J. Lee, F. Bijkerk, Aromatic structure degradation of single layer graphene on an amorphous silicon substrate in the presence of water, hydrogen and Extreme Ultraviolet light, *Appl. Surf. Sci.*, 427, Part B (2018) 1033–1040.
- [26] S. Vollebregt, R.J. Dolleman, H.S.J.v.d. Zant, P.G. Steeneken, P.M. Sarro, Suspended graphene beams with tunable gap for squeeze-film pressure sensing, in: 2017 19th International Conference on Solid-State Sensors, Actuators and Microsystems (TRANSDUCERS), 2017, pp. 770–773.
- [27] J.M. Sturm, C.J. Lee, F. Bijkerk, Reactions of ethanol on Ru(0001), *Surf. Sci.* 612 (2013) 42–47.
- [28] F. Liu, J.M. Sturm, C. Lee, F. Bijkerk, Coexistence of ice clusters and liquid-like water clusters on Ru (0001) surface, *PCCP* 19 (2017) 8288–8299.
- [29] W.A. Soer, M.J.J. Jak, A.M. Yakunin, M. van Herpen, V.Y. Banine, Grid spectral purity filters for suppression of infrared radiation in laser-produced plasma EUV sources, in: F.M. Schellenberg, B.M. LaFontaine (Eds.) *Alternative Lithographic Technologies*, 2009.
- [30] D.I. Astakhov, W.J. Goedheer, C.J. Lee, V.V. Ivanov, V.M. Krivtsov, K.N. Koshelev, D.V. Lopaev, R.M. van der Horst, J. Beckers, E.A. Osorio, F. Bijkerk, Exploring the electron density in plasma induced by EUV radiation: II. Numerical studies in argon and hydrogen, *J. Phys. D: Appl. Phys.* 49 (2016) 295204.
- [31] E.R. Kieft, J.J.A.M. van der Mullen, G.M.W. Kroesen, V. Banine, Time-resolved pinhole camera imaging and extreme ultraviolet spectrometry on a hollow cathode discharge in xenon, *Phys. Rev. E* 68 (2003) 056403.
- [32] L.G. Cancado, A. Jorio, E.H. Ferreira, F. Stavale, C.A. Achete, R.B. Capaz, M.V. Moutinho, A. Lombardo, T.S. Kulmala, A.C. Ferrari, Quantifying defects in graphene via Raman spectroscopy at different excitation energies, *Nano Lett.* 11 (2011) 3190–3196.
- [33] Y. Yamamura, J. Bohdansky, Few collisions approach for threshold sputtering, *Vacuum* 35 (1985) 561–571.
- [34] R.M. Silverstein, G.C. Bassler, T.C. Morrill, *Spectrometric Identification of Organic Compounds*, John Wiley, New York, 1991.
- [35] W.T.E. van den Beld, M. Odijk, R.H.J. Vervuurt, J.W. Weber, A.A. Bol, A. van den Berg, J.C.T. Eijkel, In-situ Raman spectroscopy to elucidate the influence of adsorption in graphene electrochemistry, *Sci. Rep.* 7 (2017) 45080.
- [36] P.J. Cumpson, M.P. Seah, Elastic scattering corrections in AES and XPS. II. Estimating attenuation lengths and conditions required for their valid use in overlayer/substrate experiments, *Surf. Interface Anal.* 25 (1997) 430–446.
- [37] A. Gao, E. Zoethout, J.M. Sturm, C.J. Lee, F. Bijkerk, Defect formation in single layer graphene under extreme ultraviolet irradiation, *Appl. Surf. Sci.* 317 (2014) 745–751.
- [38] Y. Lin, D.C. Joy, A new examination of secondary electron yield data, *Surf. Interface Anal.* 37 (2005) 895–900.
- [39] M. Alberti, R. Ayouchi, S.R. Bhattacharyya, N. Bundaleski, A. Moutinho, O. Teodoro, L. Aguilera, M. Taborelli, R. Schwarz, Secondary electron emission yield (SEY) in amorphous and graphitic carbon films prepared by PLD, in: Y. Dappe, P. Jelinek, V. Chab (Eds.) *Physica Status Solidi C: Current Topics in Solid State Physics*, Vol 9, No 6, 2012, pp. 1501–1503.